JCB Article

# Synaptotagmins are trafficked to distinct subcellular domains including the postsynaptic compartment

**Bill Adolfsen, Sudipta Saraswati, Motojiro Yoshihara, and J. Troy Littleton**

The Picower Center for Learning and Memory, Department of Biology and Department of Brain and Cognitive Sciences, Massachusetts Institute of Technology, Cambridge, MA 02139

The synaptotagmin family has been implicated in calcium-dependent neurotransmitter release, although Synaptotagmin 1 is the only isoform demonstrated to control synaptic vesicle fusion. Here, we report the characterization of the six remaining synaptotagmin isoforms encoded in the *Drosophila* genome, including homologues of mammalian Synaptotagmins 4, 7, 12, and 14. Like Synaptotagmin 1, Synaptotagmin 4 is ubiquitously present at synapses, but localizes to the postsynaptic compartment. The remaining isoforms were not found at synapses (Synaptotagmin 7), expressed at very low levels (Synaptotagmins 12 and 14), or in subsets of putative neurosecretory cells (Synaptotagmins α and β). Consistent with their distinct localizations, overexpression of Synaptotagmin 4 or 7 cannot functionally substitute for the loss of Synaptotagmin 1 in synaptic transmission. Our results indicate that synaptotagmins are differentially distributed to unique subcellular compartments. In addition, the identification of a postsynaptic synaptotagmin suggests calcium-dependent membrane-trafficking functions on both sides of the synapse.

## Introduction

Neurotransmitter release is tightly regulated by intracellular calcium levels and requires SNARE complex assembly and disassembly. The search for calcium receptors that regulate SNARE-dependent fusion has focused on the synaptotagmins, a family of transmembrane proteins containing tandem calcium-binding C2 domains (for review see Jahn et al., 2003; Koh and Bellen, 2003; Yoshihara et al., 2003). Synaptotagmin 1 (Syt 1) was identified as an abundant synaptic vesicle integral membrane protein with calcium-dependent phospholipid binding properties (Perin et al., 1990). Genetic studies in *Drosophila melanogaster* and mice have demonstrated that loss of Syt 1 specifically eliminates the fast synchronous component of release, without removing the slow asynchronous component (Geppert et al., 1994; Yoshihara and Littleton, 2002). Mutations in *syt 1* also disrupt the fourth order calcium dependence of synchronous fusion, suggesting Syt 1 functions as the presynaptic calcium sensor for fast synchronous release (Littleton et al., 1994; Fernàndez-Chacòn et al., 2001; Yoshihara and Littleton, 2002; Stevens and Sullivan, 2003).

Apart from Syt 1, more than a dozen additional synaptotagmins have been identified in mammals (Südhof, 2002), whereas the *Caenorhabditis elegans* and *Drosophila melanogaster* genomes encode eight and seven synaptotagmin genes, respectively (Lloyd et al., 2000; Adolfsen and Littleton, 2001). Several observations suggest that different synaptotagmin isoforms might cooperate to regulate the same exocytotic process, including dense core vesicle fusion in PC12 cells (Saegusa et al., 2002; Tucker et al., 2003). Heterooligomerization of distinct synaptotagmins has also been hypothesized to regulate the calcium sensitivity of neurotransmitter release (Littleton et al., 1999; Desai et al., 2000; Wang et al., 2001). Alternatively, each synaptotagmin isoform may participate in distinct membrane trafficking pathways. Supporting this model, several synaptotagmin isoforms do not colocalize with Syt 1 (Butz et al., 1999; Martinez et al., 2000; Ibata et al., 2002). To investigate the possibility that other synaptotagmins are involved in regulating neurotransmitter release, we characterized the seven synaptotagmins encoded in the *Drosophila* genome. We find that synaptotagmin isoforms localize to nonoverlapping subcellular compartments, suggesting that they participate in the regulation of distinct membrane trafficking steps in vivo.

The online version of this article includes supplemental material.

Address correspondence to J. Troy Littleton, The Picower Center for Learning and Memory, Massachusetts Institute of Technology, E18-672, 50 Ames St., Cambridge, MA 02139. Tel.: (617) 452-2605. Fax: (617) 452-2249. email: troy@mit.edu

Key words: synaptic transmission; exocytosis; *Drosophila*; membrane trafficking; C2 domain

Abbreviations used in this paper: CNS, central nervous system; EJP, excitatory junctional potential; LBD, lateral bipolar dendritic; NMJ, neuromuscular junction; VNC, ventral nerve cord.

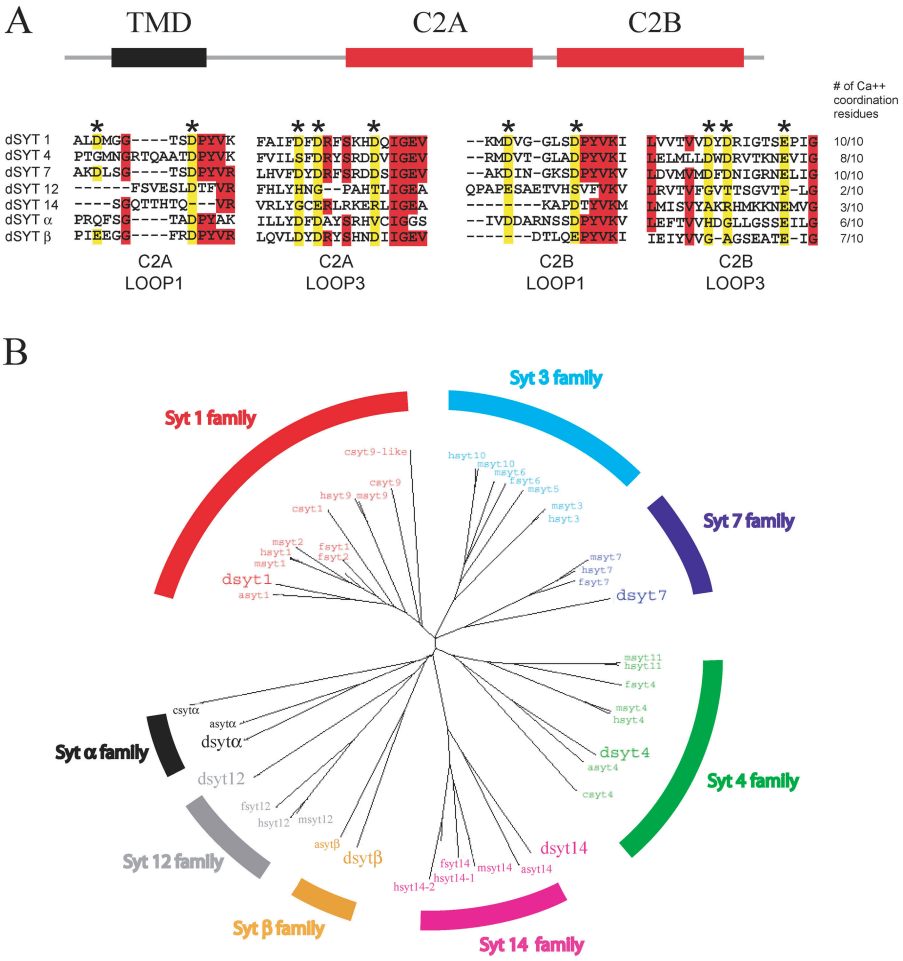


Figure 1. **Conservation of *Drosophila* synaptotagmins.** (A) The domain structure of *Drosophila* synaptotagmins is shown (top). Protein sequence alignment of loops 1 and 3 reveals the conservation of the calcium-coordinating aspartic or glutamic acid residues (*) among family members (bottom). TMD, transmembrane domain. (B) Dendrogram of synaptotagmins collected from *Drosophila*, *C. elegans*, *A. gambiae*, *F. rubripes*, *M. musculus*, and *H. sapiens* (d, c, a, f, m, and h, respectively). Subfamilies are indicated by separate colors and named according to the mammalian nomenclature. Subfamilies not containing vertebrate representatives were designated with Greek letters. Subfamilies were defined by major branches in the diagram and consist of members that are more highly conserved across different species than to other members within a particular species.

## Results

### Identification of *Drosophila* synaptotagmins and their evolutionary conservation

Taking advantage of the recently completed *Drosophila* genome, putative synaptotagmin genes have been identified using BLAST analysis with known mammalian synaptotagmin isoforms (Adams et al., 2000; Lloyd et al., 2000; Adolfsen and Littleton, 2001). Seven synaptotagmin isoforms are present in the fly genome and show a conserved domain structure consisting of an $NH_2$-terminal transmembrane domain followed by tandem C2 domains. A comparison of the amino acid sequence encompassing the negatively charged residues important for calcium coordination within each C2 domain is shown in Fig. 1 A. Only the Syt 1 and Syt 7 isoforms encode all the coordination residues for both C2 domains. Three of the remaining isoforms (Syt 4, Syt α, and Syt β) display at least 60% conservation of these charged residues, while two isoforms (Syt 12 and Syt 14) show significant divergence (Fig. 1 A), suggesting that the function of some synaptotagmins may not require calcium binding.

To determine the relationship between *Drosophila* and other metazoan synaptotagmin isoforms, we performed a cluster analysis of the predicted synaptotagmin proteins encoded in currently sequenced genomes. Synaptotagmin sequences were collected from the *C. elegans* (*C. elegans* Sequencing Consortium, 1998), *Anopheles gambiae* (Holt et al., 2002), *Fugu rubripes* (Aparicio et al., 2002), *Mus musculus* (Waterston et al., 2002), and *Homo sapiens* (Lander et al., 2001) genomes and aligned using ClustalW analysis software. Our analysis suggests the synaptotagmin superfamily can be divided into eight subfamilies based on sequence relationships across species (Fig. 1 B). The Syt 1, Syt 4, Syt 7, Syt 12, and Syt 14 subfamilies contain at least one *Drosophila* member and one or more mammalian homologues. Isoforms of the Syt 1 and Syt 4 families were identified in all vertebrate and invertebrate genomes, suggesting that these two synaptotagmin families mediate an evolutionarily conserved function required in all animals. The Syt 7, Syt 12, and Syt 14 subfamilies contain *Drosophila* and vertebrate members, but lack homologues in other invertebrate genomes. Similar to the *Drosophila* homologues, the mammalian 12 and 14 isoforms lack the majority of consensus calcium binding aspartate residues, whereas Syt 7 contains highly conserved calcium binding sites. The three remaining synaptotagmin subfamilies are not highly conserved across evolution. The Syt 3 family consists of only vertebrate members, including the mammalian 3, 5, 6, and 10 isoforms. In contrast to the Syt 3 family, the Syt α and Syt β subfamiles do not contain any obvious vertebrate orthologues.

### Expression analysis of *Drosophila* synaptotagmin mRNAs

To characterize the expression profile of the *Drosophila* synaptotagmin family, we assayed their mRNA abundance and

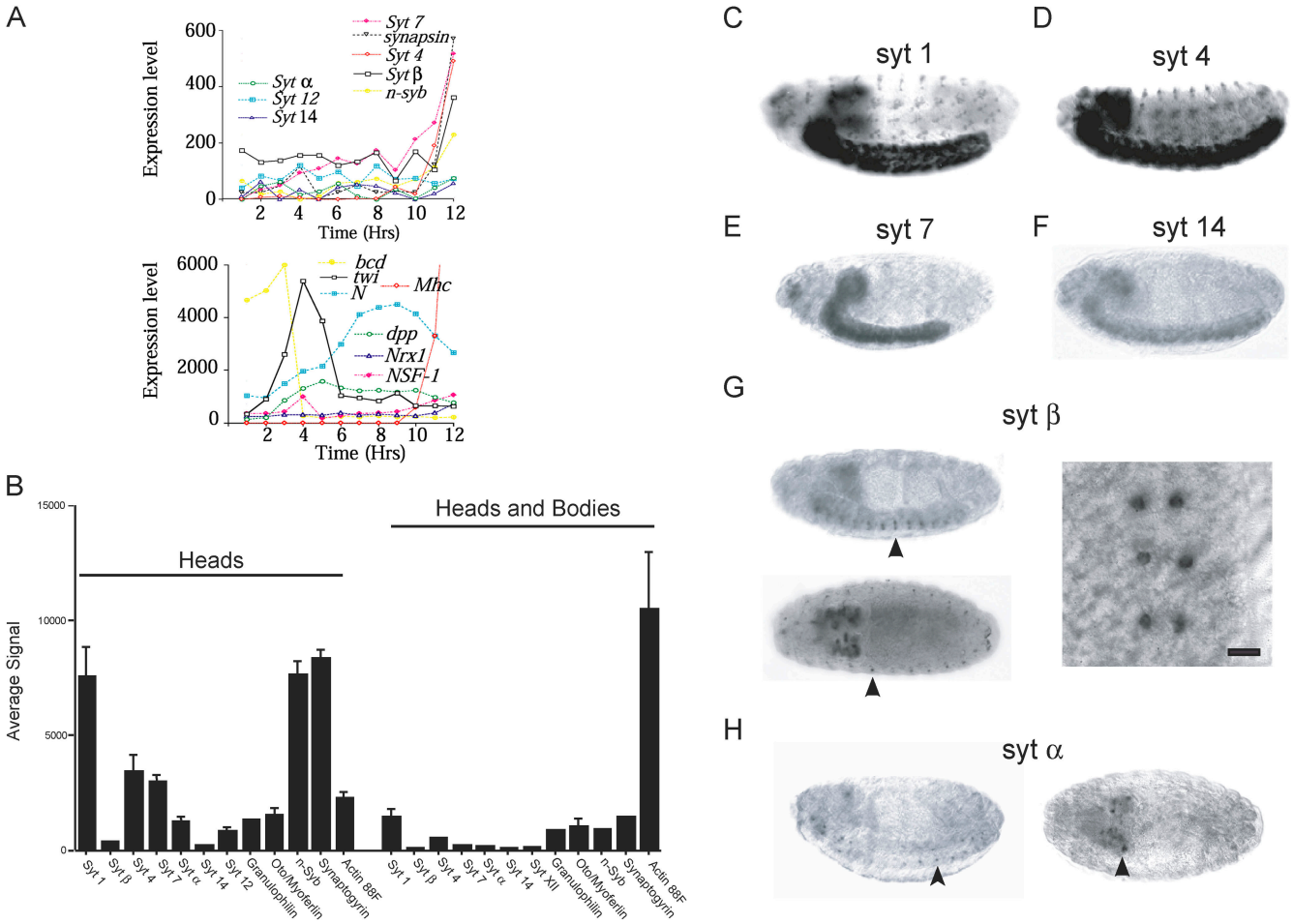


Figure 2. **Expression analysis of the *Drosophila* synaptotagmin family.** (A) Developmental microarrays conducted by the Berkeley Drosophila Genome Project are shown. (top) RNA expression levels for the *Drosophila* synaptotagmins from 0–12 h after egg-laying as detected by Affymetrix microarray quantification. (bottom) Positive controls for developmentally expressed genes are shown. (B) Relative expression levels of the *Drosophila* synaptotagmins were determined by quantitative microarray analysis of either adult Canton S heads and bodies or heads only. All synaptotagmins were enriched in heads, with *syt 1*, syt *4*, and *syt 7* being the most abundant isoforms. Error bars represent SD. Embryonic expression patterns for the synaptotagmins were determined using RNA in situ hybridization on 0–22-h embryos. (C) *syt 1* was abundantly expressed throughout the central and peripheral nervous systems. Similar to *syt 1*, *syt 4* (D) and *syt 7* (E) were expressed throughout the central and peripheral nervous systems. In addition to the CNS, *syt 7* was observed in nonneuronal tissues. (F) *syt 14* was expressed at a relatively low level in the CNS. (G) Abundant *syt* β signal was detected in a bilaterally symmetric population of large cells in the VNC (top left, arrowhead) and a subset of cells in the embryonic brain (bottom left). (right) High magnification view of the VNC cells is shown. Bar, 25 μm. Apart from cells in the nervous system, the *syt* β probe also detected several peritracheal cells (bottom left, arrowhead) present in each segment. (H) *syt* α expression was detected in a population of relatively small cells (left, arrowhead) in the VNC and a subset of cells in the brain (right, arrowhead).

localization. The abundance of mRNA transcripts and their temporal expression in embryos was determined from developmental microarray expression experiments performed by the Berkeley Drosophila Genome Project. Embryonic mRNA was isolated at 1-h windows throughout the first 12 h of development and used to probe Affymetrix *Drosophila* genome arrays that include all seven *Drosophila* synaptotagmin isoforms (Fig. 2 A). The onset of expression of *syt 1* coincides with formation of the nervous system. Similarly, none of the remaining synaptotagmins show a peak of expression before 11 h AEL, making it unlikely that they function at earlier stages of development. *syt 4*, *syt 7*, and *syt* β mRNA showed a similar developmental regulation, with increased expression from 10 to 12 h during nervous system development. The mRNAs for *syt 12*, *syt 14*, and *syt* α were expressed at very low levels throughout embryonic development.

To compare the expression levels between adults and embryos, we performed quantitative microarray analysis using Affymetrix genome arrays and mRNAs isolated from whole animals or from heads only (greatly enriching for neuronal transcripts). *syt 1* was the most abundant synaptotagmin transcript, enriched in heads (Fig. 2 B). *syt 4* and *syt 7* mRNAs were also relatively abundant, whereas the remaining synaptotagmin mRNAs were expressed at low levels, suggesting low abundance or restricted patterns of expression. None of the synaptotagmins showed increased expression in whole animal versus head extracts, suggesting that preferential enrichment of the isoforms in nonneuronal tissue is unlikely.

To identify the expression patterns for the synaptotagmin family, we performed RNA in situ hybridization experiments on 0–22-h embryos using RNA probes specific to each iso-

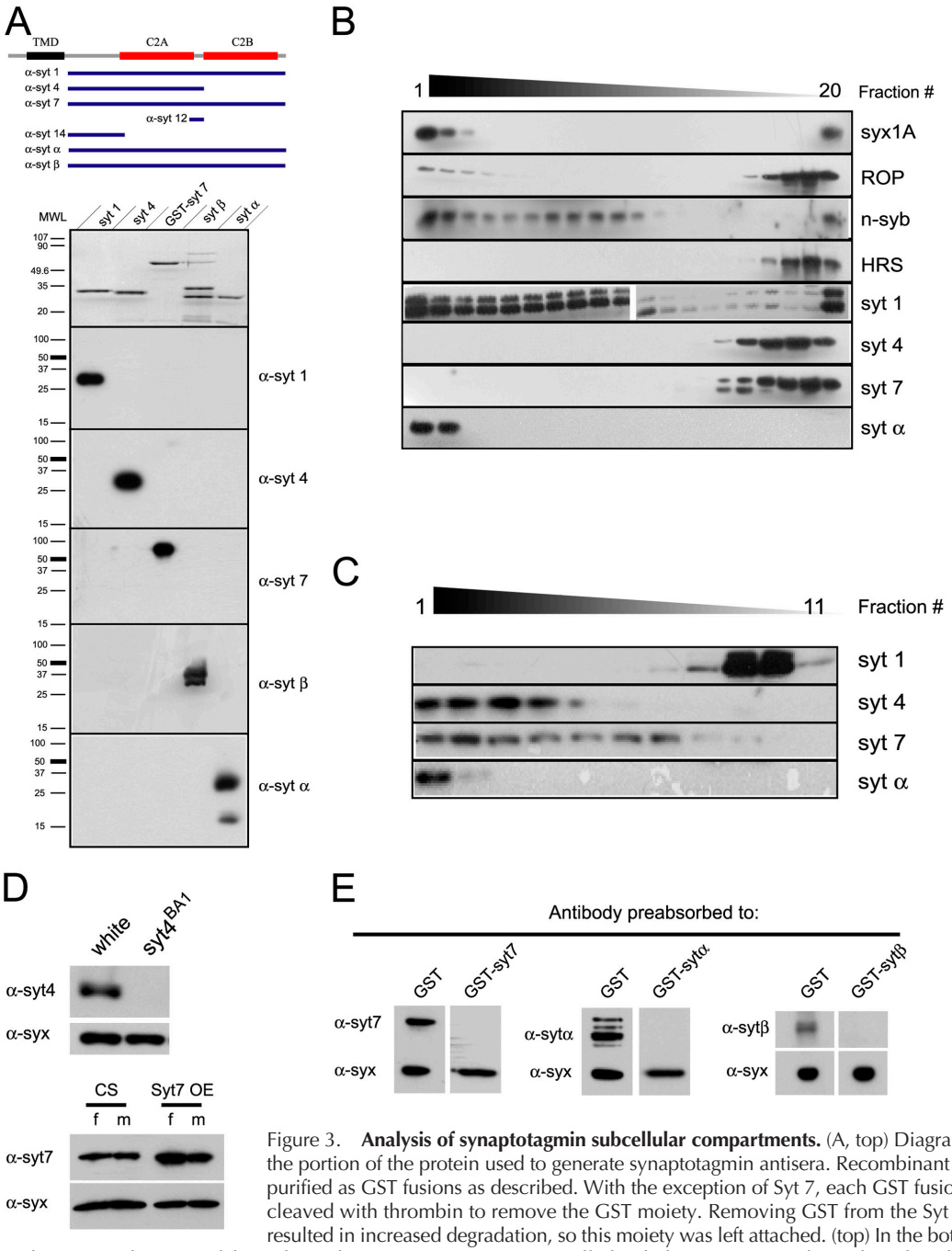


Figure 3. **Analysis of synaptotagmin subcellular compartments.** (A, top) Diagram indicating the portion of the protein used to generate synaptotagmin antisera. Recombinant proteins were purified as GST fusions as described. With the exception of Syt 7, each GST fusion protein was cleaved with thrombin to remove the GST moiety. Removing GST from the Syt 7 C2 domains resulted in increased degradation, so this moiety was left attached. (top) In the bottom portion of the diagram, recombinant C2 domains of the indicated synaptotagmins were equally loaded onto a 10% polyacrylamide gel, subjected to SDS-PAGE electrophoresis, and stained with Coomassie blue. Protein preparations were then diluted 1:20 and subjected to Western analysis with the indicated polyclonal antibodies. Each antibody is specific for the synaptotagmin isoform that served as its specific antigen. (B) Post-nuclear fractions of Canton S head extracts were separated on 10–30% sucrose gradients. Isolated fractions were probed for subcellular markers by Western analysis, including antisera against Syx1A and ROP, which localize to the plasma membrane (left-most fractions). Synaptic vesicle fractions were identified using the Syt 1 and n-Synaptobrevin antibodies, cytosolic fractions were indicated by immunostaining for ROP, and endosomal fractions by staining for HRS (Lloyd et al., 2002). Syt 4 and Syt 7 were not detected in synaptic vesicle or plasma membrane fractions, but rather found near the top of the gradient. Syt α comigrated with plasma membrane markers. The last collected fraction (right-most lane) often contained contaminants from the residual membrane debris extracted from the tube sides in the final step. (C) Equilibrium density gradient fractions were probed for synaptotagmins to detect the localization of their respective compartments. Under these conditions, synaptic vesicles (Syt 1) migrate at the top of the gradient. The remaining synaptotagmins migrated to the bottom of the gradients. (D, top) Western blots of adult head extracts collected from wild-type and a *syt 4* null mutant (*syt4*$^{BA1}$) were probed with the Syt 4 antibody. (bottom) Adult head extract isolated from either wild-type (Canton S) or animals overexpressing a *syt 7* transgene and analyzed by Western analysis using the Syt 7 antibody. Extracts were collected from females (f) (C155$^{elav\text{-}GAL4}$/+; +/+; UAS-*syt 7*/+) and males (m) (C155$^{elav\text{-}GAL4}$; +/+; UAS-*syt 7*/+) separately. (E) Specificity of the Syt 7, Syt α, and Syt β antibodies was determined using Western analysis on Canton S adult head extract. Antibodies were incubated overnight at 4°C either with sepharose beads containing the respective GST fusion proteins or GST alone. Except for the Syt β blots, which were developed at the same time, equivalent exposure times were determined by the intensity of the Syx1A signal.

form (Fig. 2, C–H). Similar to *syt 1*, *syt 4* and *syt 7* mRNAs were abundantly expressed throughout the central nervous system (CNS; Fig. 2, D and E). In addition to CNS staining, *syt 7* mRNA was expressed in several tissues outside the nervous system, indicating a more ubiquitous expression pattern. *syt 14* was expressed at low levels in the CNS (Fig. 2 F). *syt* α and *syt* β displayed a highly restricted expression pattern in subsets of CNS cells. *syt* β was expressed in a few bilaterally symmetrical large cells found in each segment of the ventral nerve cord (VNC; Fig. 2 G). Expression was also detected in peritracheal cells and within a small population of neurons in each brain lobe. The *syt* α isoform was found in a distinct population of smaller cells within each VNC segment, and in a subset of neurons within each brain lobe (Fig. 2 H). *syt 12* mRNA was not detected by microarray or in situ analysis, suggesting it is expressed at levels below detection. Together with the microarray analysis, our data indicate that Syt 1 and Syt 4 are expressed in most, if not all, neurons. Syt 7 is also abundantly expressed, but in a ubiquitous pattern both within and outside of the nervous system. The remaining synaptotagmins display restricted expression in the nervous system, labeling only specific subpopulations of cells.

### Generation of antisynaptotagmin antisera and characterization of compartmental localization

We had previously generated antisera to *Drosophila* Syt 4 and found the antisera recognized an antigen copurifying with synaptic vesicles and coIPing with Syt 1, leading us to conclude that Syt 4 was a synaptic vesicle protein (Littleton et al., 1999). The lack of a mutant in *syt 4* prevented us from confirming the antibody was isoform specific. It is now clear that the original Syt 4 antisera is not isoform specific, as the antigen detected by the antisera is not removed in animals lacking the *syt 4* locus, resulting in cross reactivity with the synaptic vesicle-localized Syt 1 protein. Therefore, to define the subcellular localization of the *Drosophila* synaptotagmins, we generated isoform-specific antisera to each synaptotagmin using multiple host animals and performed control experiments to confirm their specificity. The reactivity of the purified antisera to *Drosophila* synaptotagmins is shown in Fig. 3 A. The synaptotagmin antisera uniquely recognize their respective recombinant proteins and do not cross-react with other isoforms. In addition, preincubation of the antisera with excess recombinant antigen abolished the signal obtained on Westerns (Fig. 3 E) and immunostaining (Fig. S1, available at http://www.jcb.org/cgi/content/full/jcb.200312054/DC1). Further confirmation that the anti–Syt 7 antibody is specific was obtained by generating UAS-*syt 7* transgenic animals and overexpressing the protein using *elav*-GAL4. Overexpression of Syt 7 resulted in up-regulation of the signal detected by anti–Syt 7 antisera. The most definitive confirmation of isoform specificity is to demonstrate that immunoreactivity is lost in mutant animals. This has been determined for our antisera to Syt 1 and Syt 4, proving that these antisera display isoform specificity (Fig. 3 D and Fig. 4 B). We have not yet generated mutations in the remaining synaptotagmins, so their specificity is still tentative using these rigorous requirements. However, as shown in Fig. 6 and Fig. 7, the localization patterns for each isoform are unique and correspond with in situ results.

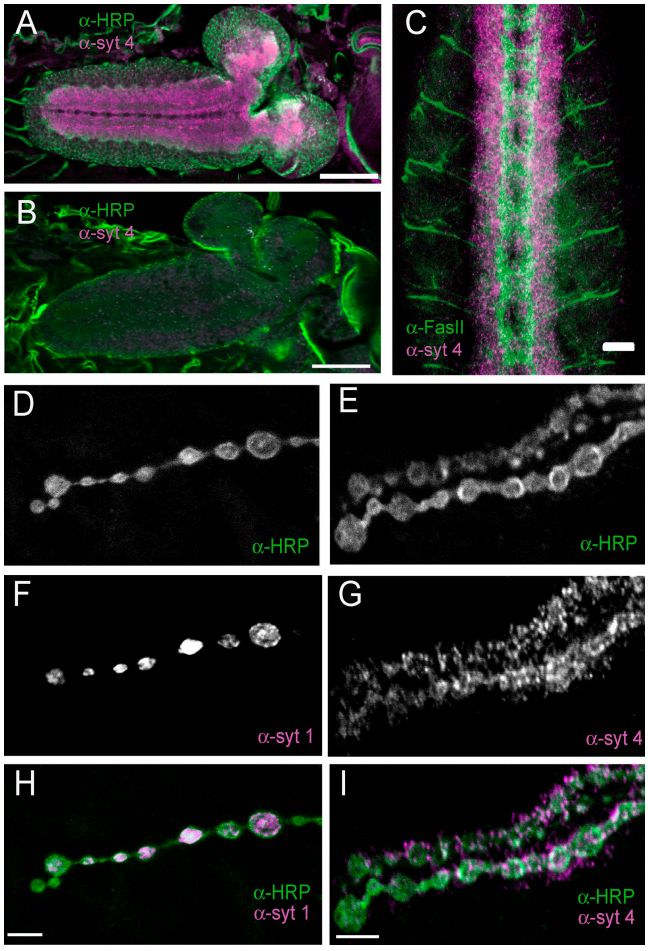


Figure 4. **Characterization of Syt 4 immunoreactivity.** (A) Wild-type first instar CNS immunostained with anti–Syt 4 (magenta) and a neuronal marker, anti-HRP (green). Bar, 50 μm. Syt 4–specific signal was concentrated in the neuropil of the ventral ganglion where synapses occur. (B) First instar CNS of a *syt 4* deletion mutant immunostained with anti–Syt 4 (magenta) and a neuronal marker, anti-HRP (green) reveals a loss of Syt 4 immunoreactivity. Bar, 50 μm. (C) Early stage 17 embryo costained with anti–Syt 4 and anti-Fas II antibodies. Bar, 20 μm. Fas II is found in axonal tracts in the CNS, whereas Syt 4 was localized to CNS cell bodies. (D–I) Wild-type third instar neuromuscular synapses were imaged after costaining with anti-HRP and either anti–Syt 1 (D, F, and H) or anti–Syt 4 (E, G, and I). Bars, 5 μm. In contrast to Syt 1 staining, which labels synaptic vesicles localized within anti-HRP labeling of the presynaptic membrane, Syt 4 immunoreactivity is found in punctate clusters localized postsynaptically outside of anti-HRP labeling.

To characterize the compartmental localization of synaptotagmins, we determined their subcellular distribution on gradients prepared from *Drosophila* brain homogenates. We performed velocity gradient subcellular fractionation experiments using 10–30% sucrose gradients to separate Canton-S head extracts. Fractions containing plasma membrane, synaptic vesicle, and cytosol compartments were identified using known markers (Syntaxin 1A [Schulze et al., 1995], n-Synaptobrevin [DiAntonio et al., 1993], and ROP [Salzberg et al., 1993]). As shown in Fig. 3 B, Syt 1 comigrates with other synaptic vesicle proteins such as n-Synaptobrevin. In contrast, Syt 4 and Syt 7 did not comigrate with Syt 1 or plasma membrane fractions, suggesting that they reside in

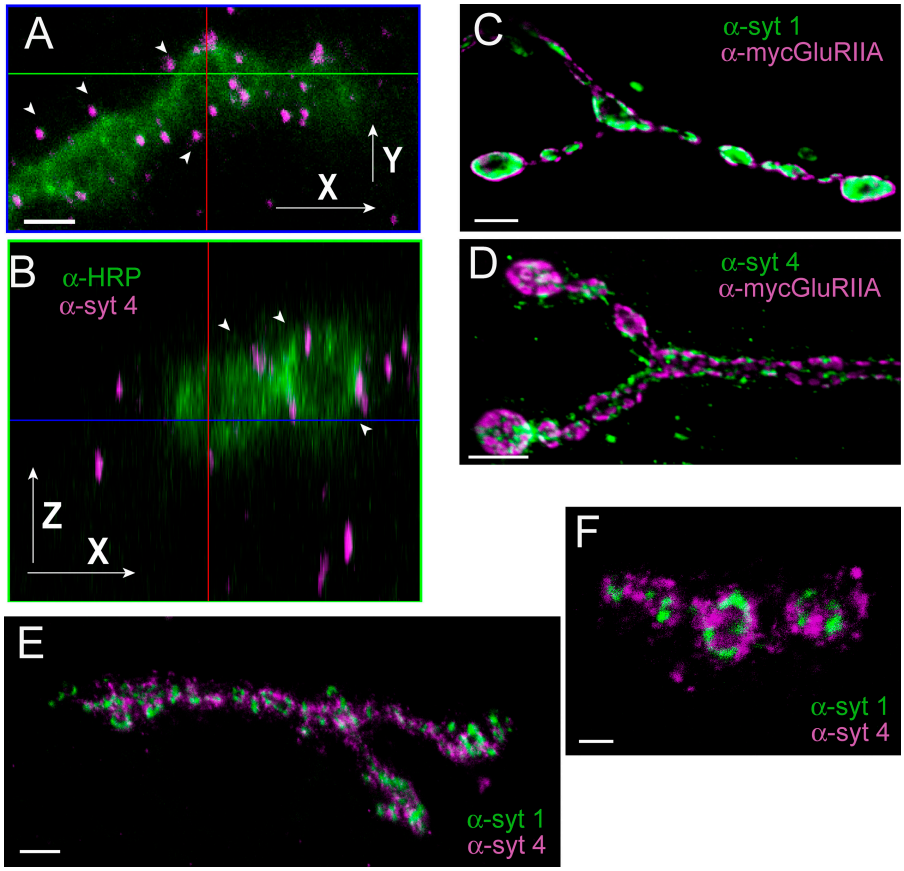


Figure 5. **Localization of Syt 4 to postsynaptic vesicles.** (A and B) Colabeling with the presynaptic membrane marker anti-HRP and anti–Syt 4. Bar, 2 μm. Confocal optical sections through a labeled third instar NMJ are shown in two axes: parallel to the body wall (X-Y; A) and perpendicular to the body wall and longitudinal (X-Z; B). Syt 4 immunoreactive clusters can be identified outside of the anti-HRP presynaptic terminal within the postsynaptic muscle (arrowheads). (C and D) Third instar neuromuscular synapses were imaged after costaining with the postsynaptic marker anti-myc antibody to detect myc-tagged GluRIIA, and either anti–Syt 1 (C) or anti–Syt 4 (D). Bar, 5 μm. Unlike Syt 1 immunoreactivity, which is found in boutons and surrounded by GluR immunoreactivity, Syt 4 concentrates at regions surrounding glutamate receptor clusters. (E and F) Colabeling with anti–Syt 1 and anti–Syt 4 in *syt 4* null mutants overexpressing UAS-syt 4 with $C155^{elav\text{-}GAL4}$. Bars: (E) 5 μm; (F) 2 μm. Although Syt 4 can be detected presynaptically when overexpressed, the Syt 4 staining is specifically excluded from Syt 1–positive synaptic vesicle domains, indicating that overexpression of Syt 4 does not cause sorting of the protein to synaptic vesicles.

compartments that are biochemically separate from Syt 1–containing synaptic vesicles. Syt α was primarily enriched in fractions containing plasma membrane proteins, and was absent from the synaptic vesicle fraction. Antibodies against Syt 14, Syt 12, and Syt β did not give a signal from brain extracts, suggesting low expression. To confirm that Syt 1–containing synaptic vesicles can be separated from other synaptotagmin compartments, we performed equilibrium density gradient centrifugation experiments using a 26% self-forming Optiprep gradient. As with velocity gradients, the Syt 1 compartment was clearly separable from the remaining synaptotagmins (Fig. 3 C). We conclude from these experiments that the remaining synaptotagmins are not present on synaptic vesicles in vivo, indicating Syt 1 is the only synaptic vesicle isoform in *Drosophila*.

## Subcellular localization of *Drosophila* synaptotagmins

To characterize the subcellular distribution of the synaptotagmins, we examined their localization in *Drosophila* embryos and larvae using immunocytochemistry. Syt 1 has been previously localized to synaptic vesicles at presynaptic terminals (Littleton et al., 1993). Similar to Syt 1 and consistent with our in situ localization data, the Syt 4 protein was found concentrated in the neuropil of the larval CNS (Fig. 4 A), suggesting localization to mature synapses. This immunostaining is abolished in mutants that remove the *syt 4* locus (Fig. 4 B). During embryonic development, the subcellular localization of Syt 4 is clearly distinct from Syt 1. As shown in Fig. 4 C, Syt 4 is abundant in neuronal cell bodies in the developing CNS at a time in which Syt 1 and other axonal markers such as Fas II have already trafficked to axons, indicating Syt 4 is differentially sorted during the establishment of neuronal polarity. The consequences of this differential sorting are apparent at mature third instar larval neuromuscular junctions (NMJs), where Syt 4, in contrast to Syt 1, is found postsynaptically (Fig. 4, D–I). Syt 4 antiserum labels the postsynaptic side of NMJs (Fig. 5, A and B), surrounding the outside of presynaptic terminals (labeled by anti-HRP) in a punctate pattern, suggesting Syt 4 resides in a postsynaptic vesicular compartment. Double labeling experiments performed in animals overexpressing a myc-tagged postsynaptic glutamate receptor subunit, mycGluRIIA, reveals that Syt 4 localizes to regions adjacent to postsynaptic receptor clusters (Fig. 5, C and D). Costaining with Syt 1 antisera demonstrates no overlap in the distribution of the two proteins, confirming Syt 4 is not a synaptic vesicle protein. In addition, overexpression of Syt 4 presynaptically in *syt 4* mutant animals does not shift its localization to synaptic vesicles (Fig. 5, E and F). Immunostaining of Syt 4 and Syt 1 revealed a nonoverlapping pattern of expression, with Syt 4 excluded from Syt 1–positive synaptic vesicle microdomains (Fig. 5 F). Although there is no overlap between Syt 4 and Syt 1 staining (Fig. 5, E and F), and the majority of Syt 4 labeling is postsynaptic (Fig. 5, A and B), a smaller fraction of Syt 4 may also localize presynaptically. However, synaptic defects present in *syt 4* mutants (unpublished data) are rescued by postsynaptic expression, suggesting that Syt 4 functions in postsynaptic trafficking steps required for synaptic growth and plasticity.

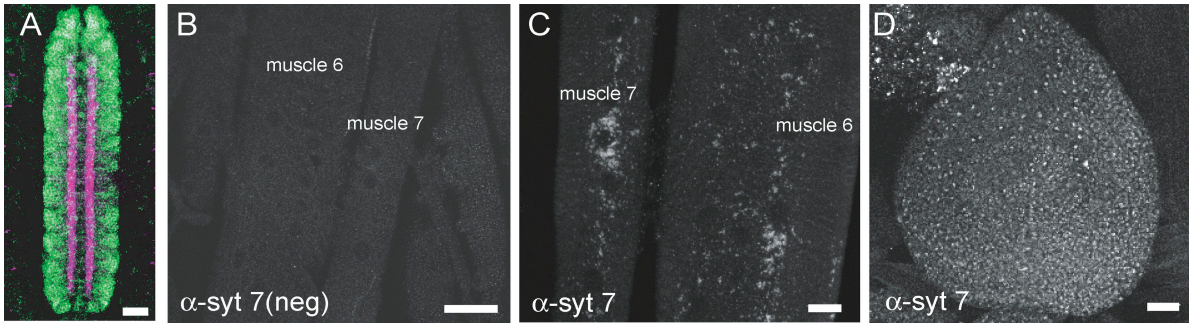


Figure 6. **Localization of *Drosophila* Syt 7.** (A) Early stage 17 embryo labeled with anti–Syt 1 (magenta) and anti–Syt 7 (green) antibodies. Bar, 20 μm. Whereas Syt 1 is localized to the synaptic neuropil, Syt 7 is found within neuronal cell bodies at this stage of development. (B) Third instar NMJ stained with anti–Syt 7 antibody preabsorbed to the recombinant GST-Syt 7 fusion protein reveals no signal. Bar, 50 μm. (C) Third instar NMJ stained with anti–Syt 7 antibody preabsorbed to recombinant GST protein reveals vesicular staining throughout the muscle at sites beneath the plasma membrane. Bar, 20 μm. (D) Third instar imaginal disc stained with anti–Syt 7 antibody reveals widespread immunolocalization of Syt 7 to cell bodies. Bar, 20 μm.

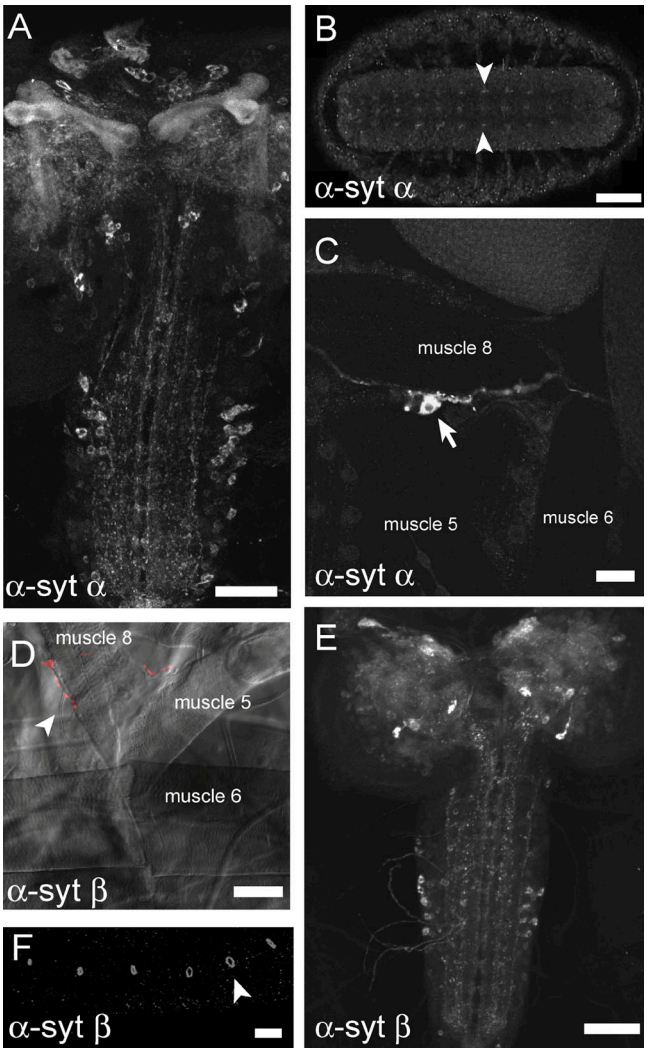


Figure 7. **Localization of *Drosophila* synaptotagmins α and β.** (A) Third instar CNS stained with the anti–Syt α antibody. Bar, 50 μm. Staining was observed in the mushroom bodies and several cell bodies in the CNS. (B) Early stage 17 embryo stained with the anti–Syt α antibody. Bar, 50 μm. Specific signal was detected in two populations of cells in the CNS, one bilaterally symmetric pair (arrowheads) and another present in the midline. (C) Third instar neuromuscular preparation stained with the anti–Syt α antibody. Signal was detected in the lateral bipolar dendritic neuron (arrow). Bar, 20 μm. (D) Syt β antibody staining of third instar NMJs. Bar, 50 μm. Fluorescence image was overlaid onto the DIC image to indicate muscle positions. Syt β staining was observed only at motor terminals innervating muscle fiber 8. (E) Third instar CNS stained with the anti–Syt β antibody. Bar, 50 μm. The antibody labels several cell bodies throughout the CNS. The immunolocalization was distinct from anti–Syt α staining, suggesting unique subpopulations of neurons expressing each isoform. (F) Staining of peritracheal cells located at tracheal branchpoints in late stage embryos is also observed with the anti–Syt β antibody, consistent with in situ labeling of the same cells. Bar, 20 μm.

Similar to Syt 4, the Syt 7 isoform was not found in axonal tracts during embryonic neuronal development, but instead localized to neuronal cell bodies (Fig. 6 A). This segregation of the synaptotagmins was maintained in mature third instar larvae. Unlike Syt 1 or Syt 4, we could not detect Syt 7 at NMJ synapses, but rather in a distinct vesicular compartment that was present not only in muscles (Fig. 6, B and C) but in other tissues, including imaginal discs (Fig. 6 D). In muscle, anti–Syt 7 staining was observed in small clusters throughout the sarcoplasm. The remaining synaptotagmin isoforms were expressed at low abundance compared with Syt 1, Syt 4, and Syt 7. Consistent with our in situ and microarray analysis, antiserum to Syt 12 and Syt 14 revealed no staining for these two isoforms in either embryos or at mature synapses in third instar larva. Syt α and Syt β were detected in subsets of neurons in the CNS and periphery that corresponded with their in situ expression patterns. In mature embryos, the Syt α protein was found in a small population of bilaterally symmetrical VNC neurons (Fig. 7 B). In third instar larvae, Syt α immunoreactivity was observed in the mushroom body and in several large CNS cell bodies (Fig. 7 A). Subsets of synaptic tracts that innervate the ventral ganglion and several ventral ganglion cell bodies were also labeled. Syt α was not detected at any peripheral motor synapses, but rather localized to the neurosecretory lateral bipolar dendritic (LBD) neuron within each abdominal segment of the larva (Fig. 7 C). Specific localization in the LBD neuron and a CNS localization pattern similar to that observed for known neuropeptides suggest Syt α may

function in trafficking of specific subclasses of neuropeptides and/or neuromodulators.

Similar to Syt α, Syt β was detected in a restricted population of cells. As observed with in situ hybridization experiments, Syt β was found in peritracheal cells that surround tracheal branchpoints in embryos (Fig. 7 F) and larvae. Syt β was also detected in several synaptic tracts and large cell bodies in the ventral ganglion. In the larval brain, Syt β immunoreactivity was absent from the mushroom bodies and instead concentrated in a pair of bilaterally symmetric cell bodies in the brain lobes that innervated the ventral ganglion. At peripheral NMJs, Syt β is present at synapses of a single motorneuron that innervates muscle fiber 8 and that release the neuropeptide leukokinin (Cantera and Nassel, 1992). In summary, our findings indicate that only the Syt 1 and Syt 4 isoforms are ubiquitously present at synapses, whereas the remaining isoforms were not detected at synapses (Syt 7), expressed at very low levels (Syt 12 and Syt 14), or in subsets of putative neurosecretory cells (Syt α and Syt β).

### Overexpression of Syt 4 and Syt 7 cannot rescue *syt 1* null mutants

The localization of synaptotagmin isoforms to distinct subcellular compartments suggests that they function in unique trafficking pathways. To test this hypothesis, we examined if Syt 4 and Syt 7, which are coexpressed in neurons with Syt 1, could rescue the synaptic transmission and behavioral defects of *syt 1* mutants when overexpressed in the nervous system. We overexpressed Syt 4 in the *syt 1* null background ($syt^{AD4}$ in trans to *Df(2L)N13*) using $C155^{elav\text{-}GAL4}$ (Fig. 8, A and B). To obtain quantitative information on the behavioral rescue, we performed larval locomotion assays to examine the output of the central motor pattern generator. Representative traces of crawling patterns from the control line $C155^{elav\text{-}GAL4}$ and the *syt 1* null mutant ($syt^{AD4}$/*Df(2L)N13*) are shown in Fig. 8 C. In contrast to the robust locomotion observed in control animals, the lack of Syt 1 dramatically slows larval locomotion. In addition to a decrease in distance traveled and locomotor cycle number (Fig. 8 D), *syt 1* null mutants display an increase in the duration of a single locomotor cycle from 1 s to ∼6 s (Fig. 8 E). Transgenic expression of the *syt 1* gene in the null background was able to partially restore all the behavioral defects observed (Fig. 8, C–E). In contrast to Syt 1, Syt 4 (Fig. 8, C–E) or Syt 7 (not depicted) overexpression did not rescue any aspect of the behavioral defects.

To directly examine synaptic transmission, we performed synaptic physiology at the third instar NMJ (Fig. 8, F–H). Consistent with previous observations, synaptic transmission was severely decreased in *syt 1* null mutants, which showed the characteristic slow rise and decay reflecting asynchronous release and a loss of the synchronous component of fusion. Overexpression of Syt 1 was able to restore evoked excitatory junctional potential (EJP) amplitudes to near wild-type levels. Similar to the lack of behavioral rescue, overexpression of Syt 4 or Syt 7 in the *syt 1* null mutant had no effect on the synaptic transmission defects. Only slow release reflecting the asynchronous component of fusion was observed in *syt 1* null mutants overexpressing Syt 4 or Syt 7, and evoked EJP amplitude was unchanged from the null mutant alone (Fig. 8 F). Our results are in disagreement with a recent work indicating that overexpression of Syt 4 using our UAS-*syt 4* construct can fully rescue synaptic transmission defects in *syt 1* mutants in *Drosophila* (Robinson et al., 2002). Their results do not fit with our observation that Syt 4 is absent from synaptic vesicles and primarily localizes postsynaptically. In addition, their results seem contradictory to the finding that the *syt 4* gene is coexpressed in all neurons with *syt 1*, yet there is a complete absence of the calcium-dependent synchronous component of release when Syt 1 is removed (Yoshihara and Littleton, 2002). To further examine these differences, we repeated our rescue experiments in saline containing 5.0 mM of extracellular calcium as previously reported (Robinson et al., 2002), but observed no rescue of the *syt 1* null phenotype by UAS-*syt 4* (Fig. 8 G). We also examined the possibility that the second chromosome *elav*-GAL4 driver used in their previous study was generating stronger expression of Syt 4 than the X chromosome $C155^{elav\text{-}GAL4}$ driver used in our rescue experiments. We generated animals containing both the X chromosome $C155^{elav\text{-}GAL4}$ and the previously used second chromosome *elav*-GAL4 to test if increased expression of Syt 4 would rescue *syt 1* mutants. We found no rescue of the *syt 1* null mutant by increased Syt 4 expression (Fig. 8 G). Instead, we observed that the increased expression of Syt 4 resulted in decreased viability. Compared with *syt 1* null mutants alone that survive to the third instar stage, there is a 96% reduction in the expected Mendelian ratios when the UAS-*syt 4* transgene is driven by both the X chromosome *elav*-GAL4 and second chromosome *elav*-GAL4 drivers. In summary, our behavioral and physiological data indicate that Syt 4 and Syt 7 cannot functionally substitute for Syt 1 when overexpressed, indicating synaptotagmins define unique membrane trafficking pathways within neurons.

## Discussion

Genetic analysis has demonstrated that Syt 1 is essential for calcium-dependent synchronous release, underlying the fourth order cooperativity of synaptic vesicle fusion, but does not abolish asynchronous calcium-dependent release (Geppert et al., 1994; Yoshihara and Littleton, 2002; Stevens and Sullivan, 2003). These observations are consistent with the current two calcium sensor model for synaptic transmission (Yamada and Zucker, 1992), with Syt 1 functioning as the calcium sensor regulating the fast synchronous component of release and an unidentified calcium sensor mediating the slow asynchronous component. Other synaptotagmin isoforms are obvious candidates for the asynchronous calcium sensor. In addition, synaptotagmins have unique calcium-binding properties (Sugita et al., 2002) and undergo heterooligomerization in vitro (Littleton et al., 1999; Desai et al., 2000). Several plasticity models have been proposed, suggesting differential expression of synaptotagmin isoforms on synaptic vesicles might regulate presynaptic release probability (Littleton et al., 1999; Wang et al., 2001) or transitions from full fusion to kiss-and-run (Wang et al., 2003). These hypotheses require that synaptotagmins have a similar expression pattern to Syt 1 and lo-

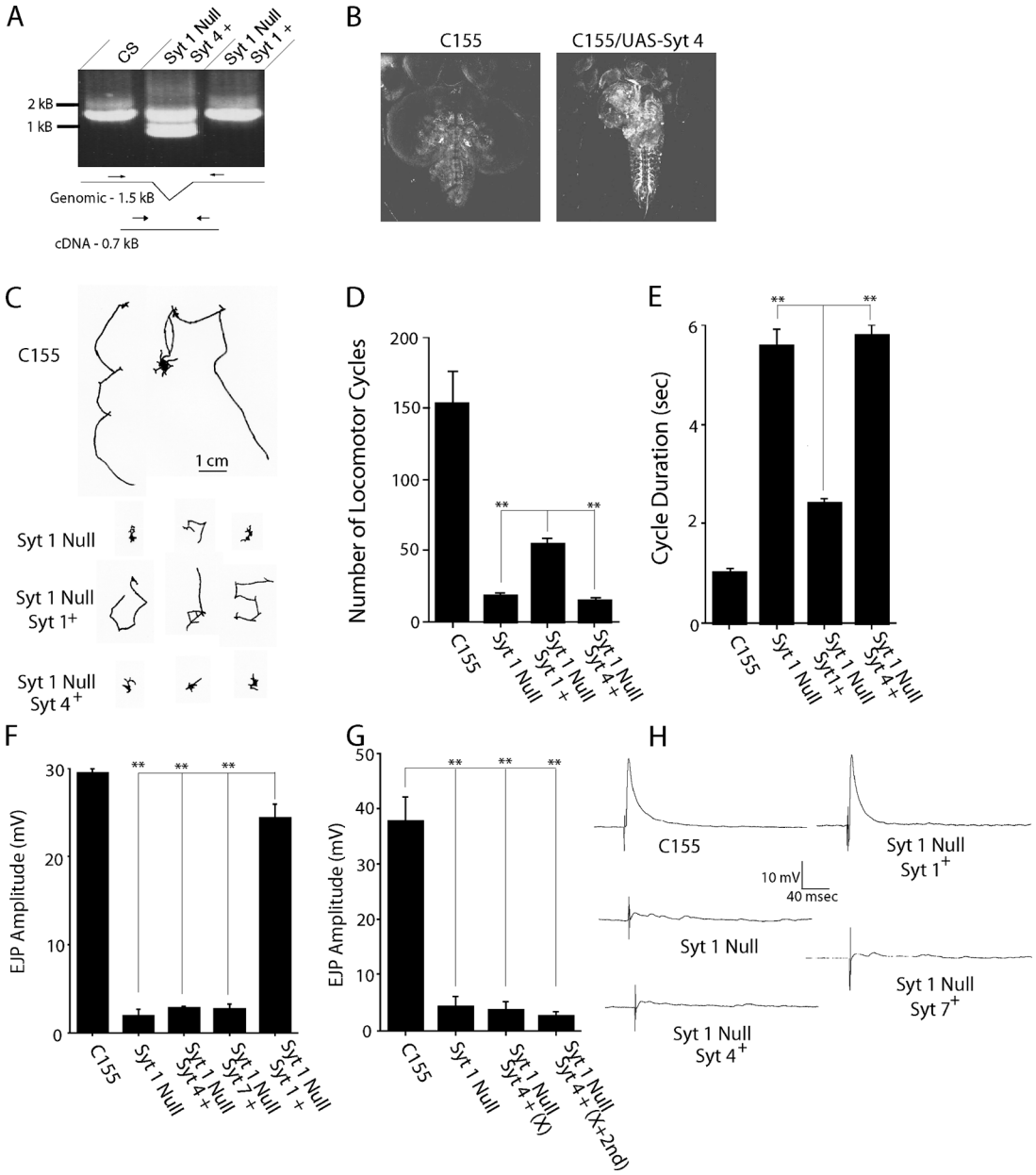


Figure 8. **Syt 4 and Syt 7 cannot rescue release defects in *syt 1* mutants.** (A) PCR confirmation of the *syt 4* transgene in animals used for rescue experiments was obtained by priming across a small intron, revealing a larger 1.5-kB band from the native genomic locus, and a 0.7-kB band specifically from animals containing the UAS-*syt 4* cDNA lacking the intron. (B) Immunostaining with anti–Syt 4 antibodies from control and C155$^{elav\text{-}GAL4}$/UAS-*syt 4*; *syt*$^{AD4}$*/Df(2L)N13* lines. The confocal settings were identical between the two pictures, and the signal intensity was set to a low level to highlight the strong up-regulation of Syt 4 in the third instar CNS of *syt 1* null animals containing UAS-*syt 4* and the C155$^{elav\text{-}GAL4}$ driver. (C) Traces of the crawling pattern of control, *syt 1* null mutants, and rescued lines containing UAS-*syt 1* or UAS-*syt 4* are shown for a 4-min imaging period. Quantification of the number of locomotor cycles during 4 min (D) and the cycle duration (E) are shown. Error bars are SEM. Similar results were observed when UAS-*syt 1* and UAS-*syt 4* were driven with a third chromosome *elav*-GAL4 driver (not depicted). The number of animals examined were as follows (number for locomotor cycle number, number for locomotor cycle duration): C155$^{elav\text{-}GAL4}$, $n = 5$, 5; *syt*$^{AD4}$*/Df(2L)N13*, $n = 17$, 7; C155$^{elav\text{-}GAL4}$/UAS-*syt 1*; *syt*$^{AD4}$*/Df(2L)N13*, $n = 15$, 5; and C155$^{elav\text{-}GAL4}$/UAS-*syt 4*; *syt*$^{AD4}$*/Df(2L)N13*, $n = 8$, 7. (F) Mean evoked EJP amplitudes (± SEM) recorded in 1.5 mM extracellular calcium for the indicated genotypes. In contrast to the rescue observed with *syt 1* transgenic expression, Syt 4 and Syt 7 had no effect on neurotransmission in the *syt 1* null mutant. Average muscle resting potentials ± SD were unchanged between the genotypes and were as follows: C155$^{elav\text{-}GAL4}$, 59.3 ± 3.9 ($n = 26$); *syt*$^{AD4}$*/Df(2L)N13*, 61.1 ± 5.2 ($n = 17$); C155$^{elav\text{-}GAL4}$/UAS-*syt 1*; *syt*$^{AD4}$*/Df(2L)N13*, 63.7 ± 3.6 ($n = 10$); C155$^{elav\text{-}GAL4}$/+; *syt*$^{AD4}$*/Df(2L)N13*; UAS-*syt 7*/+, 56.1 ± 3.4 ($n = 27$); and C155$^{elav\text{-}GAL4}$/UAS-*syt 4*; *syt*$^{AD4}$*/Df(2L)N13*, 61.5 ± 4.4 ($n = 16$). In 10% of animals containing the *syt 7* transgene, a small degree of rescue was observed, with evoked responses averaging ∼30% of the response observed in *syt 1* rescued control animals. The other 23 animals showed no rescue, and the results shown are pooled data from both sets of *syt 7* animals. No case of rescue was observed in UAS-*syt 4* overexpression experiments. (G) Mean evoked EJP amplitudes (± SEM) recorded in 5.0 mM extracellular calcium for the indicated genotypes. Average muscle resting potentials ± SD were unchanged between the genotypes and were as follows: C155$^{elav\text{-}GAL4}$, 62.1 ± 4.2 ($n = 25$); *syt*$^{AD4}$*/Df(2L)N13*, 59.4 ± 3.8 ($n = 18$); C155$^{elav\text{-}GAL4}$/UAS-*syt 4*; *syt*$^{AD4}$*/Df(2L)N13*, 57.2 ± 3.8 ($n = 26$); and C155$^{elav\text{-}GAL4}$/UAS-*syt 4*; *elav*-GAL4, *syt*$^{AD4}$*/Df(2L)N13*, 59.3 ± 4.0 ($n = 5$). (H) Representative traces of evoked responses at 1.5 mM extracellular calcium for the indicated genotypes. In contrast to the fast release observed in control and Syt 1 rescued animals, Syt 4 and Syt 7 rescued animals and the *syt 1* null mutant showed only slow EJPs, reflecting asynchronous synaptic transmission. Statistical significance was determined by *t* test; **, $P < 0.001$.

calize presynaptically at synaptic terminals. We have addressed these hypotheses in vivo by performing an extensive expression and localization study of the entire synaptotagmin family in *D. melanogaster*. Our localization data argue against the possibility that other synaptotagmin isoforms function with Syt 1 to regulate neurotransmitter release. Instead, the remaining synaptotagmin isoforms likely regulate distinct membrane trafficking steps in vivo.

Syt 4 was found in the postsynaptic compartment, suggesting it regulates a postsynaptic membrane trafficking pathway. We cannot rule out that a small fraction of Syt 4 may also be present in some presynaptic compartments, though it does not localize to Syt 1–positive synaptic vesicles. The detection of the Syt 4 protein by Western analysis and immunocytochemistry with our new antisera is abolished in *syt 4* null mutants, confirming the antisera accurately reflects the subcellular localization of Syt 4. These results indicate that previous detection of Syt 4 on synaptic vesicles (Littleton et al., 1999) reflected cross-reactivity of the old antisera with Syt 1. Given that Syt 4 does not colocalize on Syt 1–positive synaptic vesicles, the reduction of neurotransmitter release by Syt 4 up-regulation observed in *Drosophila* (Littleton et al., 1999) is unlikely to be due to heteromultimerization of the two proteins on vesicles and may instead reflect competitive binding to Syt 1 effectors or altered presynaptic calcium buffering.

In terms of Syt 4's postsynaptic localization, there is evidence in several experimental systems for a regulated form of postsynaptic vesicular trafficking (Ludwig et al., 2002). Studies in hippocampal culture neurons indicate that long-term labeling with FM1–43 loads dendritic organelles that undergo rapid calcium-triggered exocytosis that is blocked by tetanus toxin (Maletic-Savatic and Malinow, 1998). In addition, pharmacological blockage of postsynaptic membrane fusion reduces LTP (Lledo et al., 1998), suggesting postsynaptic vesicle trafficking contributes to synaptic plasticity. Mammalian Syt 4 has been localized within dendrites and soma (Ibata et al., 2002), suggesting Syt 4 and the related homologue Syt 11 may also function postsynaptically. Although the exact role for regulated postsynaptic fusion remains unclear, possibilities include the release of retrograde signals, trafficking of postsynaptic receptors, and/or trafficking of synaptic cell adhesion proteins.

The remaining synaptotagmins were not ubiquitously localized to synapses. Unlike Syt 1 or Syt 4, we could not detect Syt 7 at synapses, but found it was expressed in both neuronal and nonneuronal tissues. Mammalian Syt 7 has been found in secretory lysosomes (Martinez et al., 2000) and in synaptic active zones where it has been postulated to function as a plasma membrane calcium sensor (Sugita et al., 2001). Genetic studies of Syt 7 will be required to determine if it also functions at *Drosophila* active zones. Peripheral Syt β staining was restricted to muscle fiber 8 synapses that are known to release the neuropeptide leukokinin (Cantera and Nassel, 1992). In the CNS, Syt β was observed in a pair of bilateral neurons that may be the DPM neurosecretory neurons known to secrete the amnesiac neuropeptide. The only staining outside the nervous system is detected at tracheal branch points, where a group of myomodulin-releasing neurosecretory cells are located (O'Brien and Taghert, 1998).

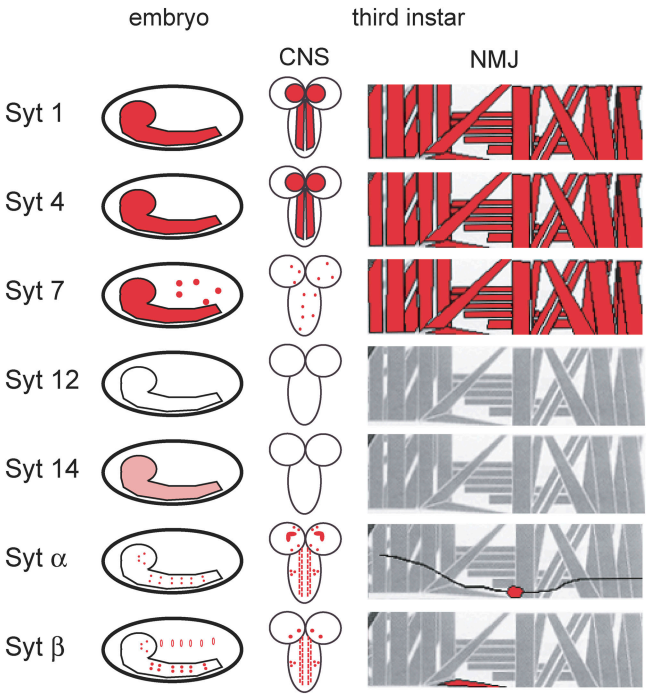


Figure 9. **Summary of the expression pattern of the *Drosophila* synaptotagmin family.** The results from embryonic in situ experiments are shown in the left panel, whereas the two right panels highlight protein expression in the third instar larval CNS and periphery. The muscles labeled red indicate NMJs where presynaptic localization of Syt 1, Syt α, or Syt β occurs, postsynaptic localization of Syt 4, and general sarcoplasmic localization of Syt 7.

These localization studies suggest Syt β is a candidate calcium sensor for mediating dense core vesicle fusion and release of neuropeptides. Similar to Syt β, Syt α showed specific expression in another set of putative CNS neuropeptide-releasing neurons, as well as within the mushroom bodies. In the periphery, staining was restricted to the LBD neurosecretory neuron, which is consistent with a role in neuropeptide release. In addition, the localization of Syt α in mushroom bodies and the possible localization of Syt β in DPM neurons makes these isoforms attractive candidates for potential roles in vesicular trafficking pathways contributing to neuronal plasticity. We were unable to localize the two remaining synaptotagmins, Syt 12 and Syt 14. It is likely that the proteins are below the detection level of our antisera, which is consistent with the microarray and in situ experiments, indicating that these isoforms are expressed at low levels in embryos and adults. Unlike the other synaptotagmins, these two isoforms lack most of the calcium coordination residues in C2A and C2B in both vertebrates and flies, indicating that they may function in trafficking pathways not regulated by calcium.

In summary, *Drosophila* synaptotagmin isoforms identify unique membrane-trafficking compartments. A summary of the expression of both the mRNA and protein for each synaptotagmin family member is shown in Fig. 9. Our data indicate that only the Syt 1 isoform is found on synaptic vesicles and so argue against heterooligomerization models. In addition, we find that Syt 4 and Syt 7 cannot rescue the behavioral or physiological defects in *syt 1* mutants, suggesting

that synaptotagmins define unique membrane trafficking pathways within neurons. It is possible synaptotagmins function in an analogous manner to control vesicle fusion, but do so in distinct compartments. Given that Syt 4 localizes to the postsynaptic compartment, our findings indicate that calcium-dependent membrane trafficking occurs on both sides of the synapse.

# Materials and methods

### Drosophila genetics

*Drosophila* were cultured on standard medium at 22°C. A null mutant in *syt 4*, *syt* $4^{BA1}$, was generated by imprecise P-element excision of EY09259, an insertion located 100 bp 5′ of the *syt 4* transcription start site. *syt* $4^{BA1}$ is an intragenic deletion that removes Syt 4 immunoreactivity. UAS-*syt 7* transgenic animals were obtained by subcloning a *syt 7* cDNA into PUAST and generating transgenic animals via standard techniques.

### Cluster analysis and dendrogram

Synaptotagmin protein sequences were collected from *Drosophila*, *C. elegans*, *A. gambiae*, *F. rubripes*, *M. musculus*, and *H. sapiens* genomes. Sequences were identified by BLAST analysis of *Drosophila* synaptotagmin protein sequences against the corresponding genomes deposited in GenBank. Collected sequences were then clustered based on homology using the ClustalW program (http://www.ch.embnet.org/software/ClustalW.html). Results were displayed as a tree diagram using the Phylodendron program (http://iubio.bio.indiana.edu/treeapp/treeprint-form.html).

### In situ hybridization

Embryos aged 0–22 h were collected and processed according to standard procedures. Probes of 500–700 bp long were designed to the C2 domain region of each synaptotagmin gene.

### Microarray analysis

Microarrays were performed with Affymetrix *Drosophila* Genechips using biotinylated cRNA using the laboratory methods described in the Affymetrix genechip expression manual (Affymetrix, Inc.). RNA was isolated from heads or heads and bodies of Canton-S males aged 3–4 d after eclosion at RT. All flies were killed between 12 and 2 p.m. to reduce any circadian-dependent transcriptional changes. Affymetrix high-density oligonucleotide arrays were probed, hybridized, stained, and washed in MIT's Biopolymers Facility according to the manufacturer's instructions. Microarray analysis was performed using Microarray Suite Vs.5 and Data Mining Tool Vs.3 statistics-based analysis software (Affymetrix, Inc.).

### Western analysis

Western blots were done using standard laboratory procedures. All synaptotagmin antibodies were used at a 1:1,000 dilution and detected using a goat anti–rabbit antibody conjugated to HRP (Jackson ImmunoResearch Laboratories). Visualization of HRP was accomplished using a SuperSignal ECL kit (Pierce Chemical Co.).

### Gradient centrifugation

Isolation of Canton-S head homogenates was performed as described previously (Littleton et al., 1999). For rate-zonal sedimentation experiments, a post-nuclear extract was layered onto a 10–30% sucrose gradient and centrifuged at 50,000 RPM for 1 h in a NVT65 rotor (Beckman Coulter). 1-ml fractions were collected beginning from the bottom of the gradient and proceeding to the top. After collection, fractions were mixed with an equal volume of 2× SDS-PAGE loading buffer and probed by Western analysis. For equilibrium sedimentation experiments, post-nuclear extract was combined with a 26% Optiprep (Axis Shield) solution. The mixed sample was centrifuged at 60,000 RPM for 3.5 h in a NVT65 rotor and fractions were collected as for velocity experiments.

### Protein expression and antibody purification

Polyclonal antibodies were generated in rabbits (Invitrogen). For the Syt 4, Syt 7, Syt α, and Syt β isoforms, we generated antisera to recombinant proteins encompassing the C2 domains of each protein. For Syt 14, we prepared antisera to a recombinant protein that encompassed the linker between the TM domain and C2A. For Syt 12, we generated antisera against a peptide derived from the linker domain between C2A and C2B. Each respective sequence was cloned into pGEX vectors. Recombinant GST fusion proteins were expressed and processed in *E. coli* (BL21) according to standard laboratory protocols. The fusion proteins were purified in batch using glutathione-sepharose (Amersham Biosciences). To remove the GST affinity tag, protein samples were incubated with thrombin for 1 h at RT. Antisera was purified using affinity chromatography. The domain of each synaptotagmin was coupled to a 1-ml NHS-activated sepharose column (Amersham Biosciences). Antisera (2 ml) injection, subsequent washes, and elution from the columns were all performed on an AKTA FPLC (Amersham Biosciences). Columns were washed in 20 mM sodium phosphate and eluted with 0.1 M glycine, pH 2.7. To minimize denaturation of the antibody at low pH, the eluted fractions were immediately mixed with 1 M Tris, pH 9. Fractions containing the desired peak were concentrated using Amicon ultra centrifugal filter devices (Millipore), aliquoted, and stored at −80°C.

### Immunostaining

Embryos and larvae were immunostained as described previously (Yoshihara and Littleton, 2002; Rieckhof et al., 2003). The dilution of primary antibodies was as follows: Syt 1 (1:1,000) Syt 4 (1:500), Syt 7 (1:1,000), Syt α (1:2,000), and Syt β (1:500). To decrease background, antibodies were preabsorbed to 0–11-h embryos. Samples were washed and mounted in 70% glycerol. Cy2-conjugated goat α–rabbit secondary antibodies (Jackson ImmunoResearch Laboratories) were used at 1:200. Visualization was performed under light microscopy using a 40× oil-immersion lens. Images were taken using confocal microscopy on a microscope (model Axoplan 2; Carl Zeiss MicroImaging, Inc.) and processed with PASCAL software (Carl Zeiss MicroImaging, Inc.).

### Electrophysiology analysis

Electrophysiological analysis of wandering stage third instar larva was performed in *Drosophila* saline (70 mM NaCl, 5 mM KCl, 4 mM $MgCl_2$, 10 mM $NaHCO_3$, 5 mM Trehalose, 115 mM sucrose, and 5 mM Hepes-NaOH, pH 7.2) supplemented with either 1.5 mM or 5.0 mM $CaCl_2$ using an Axoclamp 2B amplifier (Axon Instruments, Inc.) at 22°C as described previously (Rieckhof et al., 2003).

### Larval locomotion analysis

To quantify larval locomotion, late third instar larvae grown at 25°C were collected and placed on a flat layer of 2.9% agar supplemented with grape juice. Quantification of larval locomotion parameters was performed as described previously (Saraswati et al., 2004). For quantification of cycle duration, video recording of locomotion was performed using a digital video camera (model XL1S; Canon) attached to a 16× zoom lens (field of 3 $cm^2$). Cycle duration was reconstructed offline by digitizing frame-by-frame locomotor contractions.

### Online supplemental material

The specificity of the Syt α and Syt β antibodies for immunocytochemistry is shown in Fig. S1. Online supplemental material is available at http://www.jcb.org/cgi/content/full/jcb.200312054/DC1.

We thank Mario Mikula for help with Syt 4 antisera production, Enrico Montana and Zhuo Guan for providing microarray results, and Avital Rodal and Enrico Montana for helpful discussions about the manuscript. The 8C3 antibody developed by Seymour Benzer was obtained from the Developmental Studies Hybridoma Bank under the auspices of the National Institute of Child Health and Human Development and maintained by the University of Iowa, Department of Biological Sciences, Iowa City, IA 52242.

This work was supported by grants from the National Institutes of Health, the Human Frontiers Science Program Organization, the Packard Foundation, and the Searle Scholars Program. J.T. Littleton is an Alfred P. Sloan Research Fellow.

Submitted: 5 December 2003
Accepted: 10 June 2004

# References

Adams, M.D., S.E. Celniker, R.A. Holt, C.A. Evans, J.D. Gocayne, P.G. Amanatides, S.E. Scherer, P.W. Li, R.A. Hoskins, R.F. Galle, et al. 2000. The genome sequence of *Drosophila melanogaster. Science.* 287:2185–2195.

Adolfsen, B., and J.T. Littleton. 2001. Genetic and molecular analysis of the synaptotagmin family. *Cell. Mol. Life Sci.* 58:393–402.

Aparicio, S., J. Chapman, E. Stupka, N. Putnam, J.M. Chia, P. Dehal, A. Christoffels, S. Rash, S. Hoon, A. Smit, et al. 2002. Whole-genome shotgun assembly and analysis of the genome of *Fugu rubripes. Science.* 297:1301–1310.

Butz, S., R. Fernandez-Chacon, F. Schmitz, R. Jahn, and T.C. Südhof. 1999. The subcellular localizations of atypical synaptotagmins III and VI. Synaptotagmin III is enriched in synapses and synaptic plasma membranes but not in synaptic vesicles. *J. Biol. Chem.* 274:18290–18296.

Cantera, R., and D.R. Nassel. 1992. Segmental peptidergic innervation of abdominal targets in larval and adult dipteran insects revealed with an antiserum against leucokinin I. *Cell Tissue Res.* 269:459–471.

*C. elegans* Sequencing Consortium. 1998. Genome sequence of the nematode *C. elegans:* a platform for investigating biology. *Science*. 282:2012–2018.

Desai, R.C., B. Vyas, C.A. Earles, J.T. Littleton, J.A. Kowalchyck, T.F. Martin, and E.R. Chapman. 2000. The C2B domain of synaptotagmin is a $Ca^{2+}$-sensing module essential for exocytosis. *J. Cell Biol.* 150:1125–1136.

DiAntonio, A., R.W. Burgess, A.C. Chin, D.L. Deitcher, R.H. Scheller, and T.L. Schwarz. 1993. Identification and characterization of *Drosophila* genes for synaptic vesicle proteins. *J. Neurosci.* 13:4924–4935.

Fernàndez-Chacòn, R., A. Königstorfer, S.H. Gerber, J. Garcìa, M.F. Matos, C.F. Stevens, N. Brose, J. Rizo, C. Rosenmund, and T.C. Südhof. 2001. Synaptotagmin I functions as a calcium regulator of release probability. *Nature.* 410:41–49.

Geppert, M., Y. Goda, R.E. Hammer, C. Li, T.W. Rosahl, C.F. Stevens, and T.C. Südhof. 1994. Synaptotagmin I: a major $Ca^{2+}$ sensor for transmitter release at a central synapse. *Cell.* 79:717–727.

Holt, R.A., G.M. Subramanian, A. Halpern, G.G. Sutton, R. Charlab, D.R. Nusskern, P. Wincker, A.G. Clark, J.M. Ribeiro, R. Wides, et al. 2002. The genome sequence of the malaria mosquito *Anopheles gambiae. Science.* 298: 129–149.

Ibata, K., T. Hashikawa, T. Tsuboi, S. Terakawa, F. Liang, A. Mizutani, M. Fukuda, and K. Mikoshiba. 2002. Non-polarized distribution of synaptotagmin IV in neurons: evidence that synaptotagmin IV is not a synaptic vesicle protein. *Neurosci. Res.* 43:401–406.

Jahn, R., T. Lang, and T.C. Südhof. 2003. Membrane fusion. *Cell.* 112:519–533.

Koh, T.W., and H.J. Bellen. 2003. Synaptotagmin I, a $Ca^{2+}$ sensor for neurotransmitter release. *Trends Neurosci.* 26:413–422.

Lander, E.S., L.M. Linton, B. Birren, C. Nusbaum, M.C. Zody, J. Baldwin, K. Devon, K. Dewar, M. Doyle, W. FitzHugh, et al. 2001. Initial sequencing and analysis of the human genome. *Nature.* 409:860–921.

Littleton, J.T., H.J. Bellen, and M.S. Perin. 1993. Expression of synaptotagmin in *Drosophila* reveals transport and localization of synaptic vesicles to the synapse. *Development.* 118:1077–1088.

Littleton, J.T., M. Stern, M. Perin, and H.J. Bellen. 1994. Calcium dependence of neurotransmitter release and rate of spontaneous vesicle fusions are altered in *Drosophila* synaptotagmin mutants. *Proc. Natl. Acad. Sci. USA.* 91:10888–10892.

Littleton, J.T., T.L. Serano, G.M. Rubin, B. Ganetzky, and E.R. Chapman. 1999. Synaptic function modulated by changes in the ratio of synaptotagmin I and IV. *Nature.* 400:757–760.

Lledo, P.M., X. Zhang, T.C. Südhof, R.C. Malenka, and R.A. Nicoll. 1998. Postsynaptic membrane fusion and long-term potentiation. *Science.* 279: 399–403.

Ludwig, M., N. Sabatier, P.M. Bull, R. Landgraf, G. Dayanithi, and G. Leng. 2002. Intracellular calcium stores regulate activity-dependent neuropeptide release from dendrites. *Nature.* 418:85–89.

Lloyd, T.E., P. Verstreken, E.J. Ostrin, A. Phillippi, O. Lichtarge, and H.J. Bellen. 2000. A genome-wide search for synaptic vesicle cycle proteins in *Drosophila. Neuron.* 26:45–50.

Lloyd, T.E., R. Atkinson, M.N. Wu, Y. Zhou, G. Pennetta, and H.J. Bellen. 2002. Hrs regulates endosome membrane invagination and tyrosine kinase receptor signaling in *Drosophila. Cell.* 108:261–269.

Maletic-Savatic, M., and R. Malinow. 1998. Calcium-evoked dendritic exocytosis in cultured hippocampal neurons. Part I: trans-Golgi network-derived organelles undergo regulated exocytosis. *J. Neurosci.* 18:6803–6813.

Martinez, I., S. Chakrabarti, T. Hellevik, J. Morehead, K. Fowler, and N.W. Andrews. 2000. Synaptotagmin VII regulates $Ca^{2+}$-dependent exocytosis of lysosomes in fibroblasts. *J. Cell Biol.* 148:1141–1149.

O'Brien, M.A., and P.H. Taghert. 1998. A peritracheal neuropeptide system in insects: release of myomodulin-like peptides at ecdysis. *J. Exp. Biol.* 201(Pt 2): 193–209.

Perin, M.S., V.A. Fried, G.A. Mignery, R. Jahn, and T.C. Südhof. 1990. Phospholipid binding by a synaptic vesicle protein homologous to the regulatory region of protein kinase C. *Nature.* 345:260–263.

Rieckhof, G.E., M. Yoshihara, Z. Guan, and J.T. Littleton. 2003. Presynaptic N-type calcium channels regulate synaptic growth. *J. Biol. Chem.* 278: 41099–41108.

Robinson, I.M., R. Ranjan, and T.L. Schwarz. 2002. Synaptotagmins I and IV promote transmitter release independently of $Ca^{2+}$ binding in the $C_2A$ domain. *Nature.* 418:336–340.

Saegusa, C., M. Fukuda, and K. Mikoshiba. 2002. Synaptotagmin V is targeted to dense-core vesicles that undergo calcium-dependent exocytosis in PC12 cells. *J. Biol. Chem.* 277:24499–24505.

Salzberg, A., N. Cohen, N. Halachmi, Z. Kimchie, and Z. Lev. 1993. The *Drosophila Ras2* and *Rop* gene pair: a dual homology with a yeast *Ras*-like gene and a suppressor of its loss-of-function phenotype. *Development.* 117:1309–1319.

Saraswati, S., L.E. Fox, D.R. Soll, and C.F. Wu. 2004. Tyramine and octopamine have opposite effects on the locomotion of *Drosophila* larvae. *J. Neurobiol.* 58:425–441.

Schulze, K., K. Broadie, M. Perin, and H.J. Bellen. 1995. Genetic and electrophysiological studies of *Drosophila* syntaxin-1A demonstrate its role in nonneuronal secretion and neurotransmission. *Cell.* 80:311–320.

Stevens, C.F., and J.M. Sullivan. 2003. The synaptotagmin C2A domain is part of the calcium sensor controlling fast synaptic transmission. *Neuron.* 39:299–308.

Südhof, T.C. 2002. Synaptotagmins: why so many? *J. Biol. Chem.* 277:7629–7632.

Sugita, S., W. Han, S. Butz, X. Liu, R. Fernandez-Chacon, Y. Lao, and T.C. Südhof. 2001. Synaptotagmin VII as a plasma membrane $Ca^{2+}$ sensor in exocytosis. *Neuron.* 30:459–473.

Sugita, S., O.H. Shin, W. Han, Y. Lao, and T.C. Südhof. 2002. Synaptotagmins form a hierarchy of exocytotic $Ca^{2+}$ sensors with distinct $Ca^{2+}$ affinities. *EMBO J.* 21:270–280.

Tucker, W.C., J.M. Edwardson, J. Bai, H.J. Kim, T.F. Martin, and E.R. Chapman. 2003. Identification of synaptotagmin effectors via acute inhibition of secretion from cracked PC12 cells. *J. Cell Biol.* 162:199–209.

Wang, C.T., R. Grishanin, C.A. Earles, P.Y. Chang, T.F. Martin, E.R. Chapman, and M.B. Jackson. 2001. Synaptotagmin modulation of fusion pore kinetics in regulated exocytosis of dense-core vesicles. *Science.* 294:1111–1115.

Wang, C.T., J.C. Lu, J. Bai, P.Y. Chang, T.F. Martin, E.R. Chapman, and M.B. Jackson. 2003. Different domains of synaptotagmin control the choice between kiss-and-run and full fusion. *Nature.* 424:943–947.

Waterston, R.H., K. Lindblad-Toh, E. Birney, J. Rogers, J.F. Abril, P. Agarwal, R. Agarwala, R. Ainscough, M. Alexandersson, P. An, et al. 2002. Initial sequencing and comparative analysis of the mouse genome. *Nature.* 420:520–562.

Yamada, W.M., and R.S. Zucker. 1992. Time course of transmitter release calculated from simulations of a calcium diffusion model. *Biophys. J.* 61:671–682.

Yoshihara, M., and J.T. Littleton. 2002. Synaptotagmin I functions as a calcium sensor to synchronize neurotransmitter release. *Neuron.* 36:897–908.

Yoshihara, M., B. Adolfsen, and J.T. Littleton. 2003. Is synaptotagmin the calcium sensor? *Curr. Opin. Neurobiol.* 13:315–323.